

# HNO<sub>3</sub> Forming Channel of the HO<sub>2</sub> + NO Reaction as a Function of Pressure and Temperature in the Ranges of 72–600 Torr and 223–323 K

Nadezhda Butkovskaya,\* Alexandre Kukui,<sup>†</sup> and Georges Le Bras

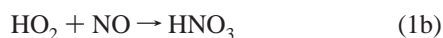
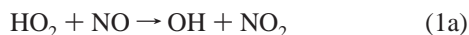
CNRS, Institut de Combustion, Aérothermique, Réactivité et Environnement (ICARE),  
1C Av. de la Recherche Scientifique, 45071 Orléans Cedex 2, France

Received: May 28, 2007; In Final Form: July 16, 2007

A high-pressure turbulent flow reactor coupled with a chemical ionization mass-spectrometer was used to determine the branching ratio of the HO<sub>2</sub> + NO reaction: HO<sub>2</sub> + NO → OH + NO<sub>2</sub> (1a), HO<sub>2</sub> + NO → HNO<sub>3</sub> (1b). The branching ratio,  $\beta = k_{1b}/k_{1a}$ , was derived from the measurements of “chemically amplified” concentrations of the NO<sub>2</sub> and HNO<sub>3</sub> products in the presence of O<sub>2</sub> and CO. The pressure and temperature dependence of  $\beta$  was determined in the pressure range of 72–600 Torr of N<sub>2</sub> carrier gas between 323 and 223 K. At each pressure, the branching ratio was found to increase with the decrease of temperature, the increase becoming less pronounced with the increase of pressure. In the 298–223 K range, the data could be fitted by the expression:  $\beta(T,P) = (530 \pm 10)/T(\text{K}) + (6.4 \pm 1.3) \times 10^{-4}P(\text{Torr}) - (1.73 \pm 0.07)$ , giving  $\beta \approx 0.5\%$  near the Earth’s surface (298 K, 760 Torr) and 0.8% in the tropopause region (220 K, 200 Torr). The atmospheric implication of these results is briefly discussed.

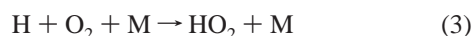
## 1. Introduction

We have recently reported the observation of a minor channel forming HNO<sub>3</sub> (1b) in the gas-phase reaction of the HO<sub>2</sub> radical with NO:<sup>1</sup>



The study was carried out in a turbulent flow reactor (TFR) coupled with a chemical ionization mass-spectrometer (CIMS). The channel (1b) was quantified by direct detection of HNO<sub>3</sub> at pressure  $P = 200$  Torr in the reactor, and a value of 0.18% was obtained for the branching ratio  $k_{1b}/k_{1a}$  at  $T = 298$  K. A negative temperature dependence was found for this branching ratio with a value of 0.9% at 223 K.

Reaction 1 is a very important atmospheric reaction. It plays a key role in controlling the interconversion between OH and HO<sub>2</sub> radicals in the troposphere through the cycle



Reaction 1a is also a major source of tropospheric ozone through the conversion of NO to NO<sub>2</sub> followed by NO<sub>2</sub> photolysis to NO and O-atoms, these latter combining with O<sub>2</sub> to produce ozone. The efficiency of the above cycle is decreased by chain termination reactions, one of the most important being



Reaction 1b is another chain termination reaction suggested to be significant in the upper troposphere.<sup>1</sup> Regarding the potential importance of reaction 1b in the whole atmosphere, it is necessary to determine the branching  $k_{1b}/k_{1a}$  over the whole ranges of atmospheric pressures and temperatures.

In the present work, measurements of the branching ratio for reaction 1 was extended to the pressure range of 72–600 Torr in the temperature range 223–323 K to provide a parametrization equation to be used to assess the role of reaction 1b in model calculations of the atmospheric composition. To increase the HNO<sub>3</sub> signal-to-noise ratio, “chemical amplification” according to reactions 1–3 was utilized in the TFR with the chain length of the order of ten. A linear pressure dependence for the branching ratio  $k_{1b}/k_{1a}$  was found, and a negative temperature dependence, previously observed at  $P = 200$  Torr,<sup>1</sup> was confirmed for the whole range of the indicated pressures between 323 and 223 K.

## 2. Experimental Section

**2.1. Chemical Reactor.** The experimental setup consisting of a high-pressure turbulent flow reactor coupled to a chemical ionization mass spectrometer was similar to that used in our first study of the HO<sub>2</sub> + NO reaction.<sup>1</sup> A scheme of the apparatus is presented in Figure 1. The flow in the TFR was created by N<sub>2</sub> carrier gas evaporating from a liquid nitrogen tank. The pressure in the TFR was controlled by regulating the throttling valve of the reactor pump and varying the main N<sub>2</sub> flow. The Reynolds numbers were in the range from 4900 to 11000 at flow rates from 64 to 145 SLPM corresponding to pressures from 70 to 600 Torr. Reactor temperature was controlled by combined effects of cooling via passing the main flow through the metal coil immersed into a Dewar with liquid N<sub>2</sub> and heating using a CB100 digital controller (RKC Instrument). This controller also allowed heating the reactor up to 50 °C.

\* Corresponding author. E-mail: bout@cnrs-orleans.fr. Permanent address: Institute of Chemical Physics of the Russian Academy of Sciences, 117334 Moscow, Russian Federation.

<sup>†</sup> CNRS, Service d’Aéronomie, IPSL, Paris.

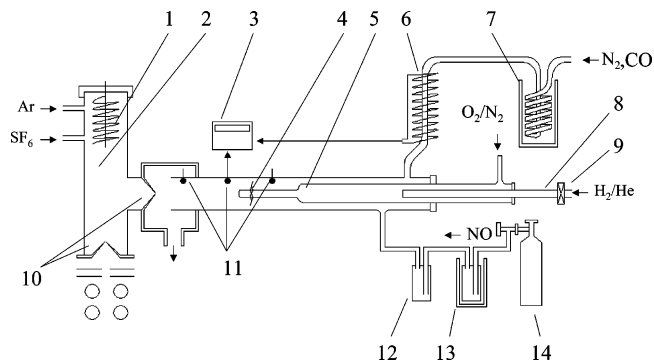
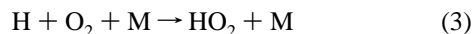


**Figure 1.** Experimental setup: 1, ion source; 2, ion-molecule reactor; 3, temperature controller; 4, «turbulizer»; 5, injector; 6, resistance; 7, cooling bath; 8, discharge tube; 9, microwave discharge; 10, sampling cones; 11, temperature sensor; 12, Fe<sup>II</sup>(SO<sub>4</sub>) filter; 13, cool bath; 14, NO cylinder.

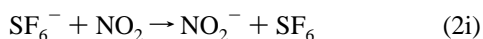
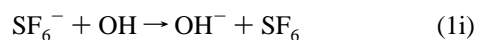
HO<sub>2</sub> radicals were produced in the TFR by the reaction



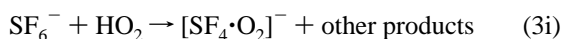
with H-atoms generated by a microwave discharge in H<sub>2</sub>/He gas mixtures flowing through a quartz tube concentrically connected to the movable injector. The flows of N<sub>2</sub> in the injector and of He in the discharge tube were optimized for maximum H-atoms production. He (AlphaGaz 2) was purified by passing through molecular sieves cooled by liquid N<sub>2</sub>. Tank grade H<sub>2</sub> (AlphaGaz 2) was used without further purification. NO was introduced into the TFR upstream of the tip of the injector. The tank grade NO (AlphaGaz N20) passed successively through ethanol/liquid nitrogen cooled traps and Fe<sup>II</sup>(SO<sub>4</sub>) filter to remove NO<sub>2</sub> and heavier nitrogen oxides. NO flow rate of about 0.6 SCCM was maintained using a TYLAN flow controller. O<sub>2</sub> (AlphaGaz 2) and CO (AlphaGaz N47) were added into the main N<sub>2</sub> stream using CELERITY flow controllers. The maximum distance from the injector tip to the orifice of the inlet cone of the ion-molecule reactor was  $L = 50$  cm, which corresponded to a reaction time in the TFR of about  $t = 30$  ms at  $P = 200$  Torr and  $T = 298$  K.

**2.2. CIMS Detection and Sensitivity.** Gas mixtures from the TFR were sampled through a Teflon cone with orifice diameter of 0.5 mm into the ion-molecule reactor (IMR) located perpendicular to the TFR. The flow rate of the Ar carrier gas in the IMR was 3.6 SLPM at the typical pressure of 0.7 Torr. The primary Ar<sup>+</sup> ions and electrons were generated in the ion source by a heated filament. The emission current from the filament was always stabilized during the measurements. SF<sub>6</sub> was continuously introduced into the IMR downstream of the ion source. The primary SF<sub>6</sub><sup>-</sup> negative ions were produced by attachment of thermalized electrons to SF<sub>6</sub>.

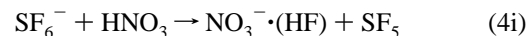
OH radicals and NO<sub>2</sub> were detected as OH<sup>-</sup> ( $m/e$  17) and NO<sub>2</sub><sup>-</sup> ( $m/e$  46) ions formed by electron transfer from SF<sub>6</sub><sup>-</sup>:<sup>2</sup>



HO<sub>2</sub> radicals were detected at  $m/e$  140 using the reaction<sup>3</sup>



HNO<sub>3</sub> was detected using the reaction with SF<sub>6</sub><sup>-</sup>, giving the peak at  $m/e$  82:<sup>4</sup>



The branching ratio of reaction 1,  $\beta = k_{1b}/k_{1a}$ , was obtained by measuring the concentration ratio of the HNO<sub>3</sub> and NO<sub>2</sub> products from channels 1b and 1a, respectively. To convert the measured intensity ratio of the products,  $\Delta I_{82}/\Delta I_{46}$ , to the concentration ratio, it is necessary to know the ratio of the apparatus sensitivities to HNO<sub>3</sub> and NO<sub>2</sub>,  $S_{\text{HNO}_3}/S_{\text{NO}_2}$ . The  $S_{\text{HNO}_3}/S_{\text{NO}_2}$  ratio and the absolute sensitivities themselves are determined by a number of parameters which vary with changing the pressure in the TFR. The most important parameters include pressure and flow velocity in the IMR, sampling conditions at the interface between the TFR and IMR, optimum potentials applied to the sampling cone, and the ion optics elements behind it. To account for the dependence of the sensitivities on the pressure in the TFR, the following approach was adopted. At  $P = 200$  Torr, the absolute and relative sensitivities were determined using a calibration method described in our previous study.<sup>1</sup> In brief, the three-step procedure consisted of (1) NO<sub>2</sub> calibration using a standard NO<sub>2</sub> gas mixture, (2) OH calibration using reaction 5 at short reaction times and low NO<sub>2</sub> concentrations, and (3) calibration of nitric acid by measuring the kinetics of the OH decay and appearance of HNO<sub>3</sub> in reaction 4:



The advantages of such “chemical” calibration are (i) in situ production of HNO<sub>3</sub> that eliminates the problems connected with the introduction of HNO<sub>3</sub> into the reactor and (ii) absence of the errors connected with the determination of NO<sub>2</sub> concentration, as these errors vanish in the sensitivity ratio  $S_{\text{HNO}_3}/S_{\text{NO}_2}$ . This procedure was also used in some experiments at  $P = 100$ , 300, 400, and 500 Torr. However, to avoid potential problems related to increasing formation of peroxyxynitrous acid, HOONO, with pressure in reaction 4<sup>5</sup> and to simplify the calibration procedure for other pressures in the TFR, the  $S_{\text{HNO}_3}/S_{\text{NO}_2}$  ratios were derived from the changes of NO<sub>2</sub> and HNO<sub>3</sub> sensitivities relative to those at 200 Torr determined from direct introduction of HNO<sub>3</sub> and NO<sub>2</sub> into the TFR.

The change of  $S_{\text{HNO}_3}$  with pressure was determined by flowing gaseous HNO<sub>3</sub> from the mixture of HNO<sub>3</sub> (Aldrich, 69%) and H<sub>2</sub>SO<sub>4</sub> (Sigma-Aldrich, 90%) aqueous solutions (10:1 volume ratio) into the reactor. Gaseous HNO<sub>3</sub> was transported by a He flow bubbling through the solution mixture in a glass trap. The trap was kept below 16 °C to avoid saturation of the HNO<sub>3</sub> signal. The helium flow was varied by means of a CELERITY mass flow controller with 10 SCCM maximum flow rate. A dilution by larger He flow regulated using a 250 SCCM TYLAN flow controller took place shortly downstream of the trap. The trap was connected to the reactor via a PFA tube. At each pressure  $S_{\text{HNO}_3}$  was determined from the linear increase of the signal intensity at  $m/e$  82 with the flow rate of He passing through the bubbler. The HNO<sub>3</sub> partial pressure over the solution,  $P_{\text{HNO}_3}$ , was not known, but this was not critical because only the sensitivities relative to those at 200 Torr,  $S_P/S_{200}$  (HNO<sub>3</sub>) =  $S_{\text{HNO}_3}(P)/S_{\text{HNO}_3}(200)$ , were used. A rough estimation using the average ratio  $S_{\text{HNO}_3}/S_{\text{NO}_2} \approx 4$  from the chemical calibration at 200 Torr gave  $P_{\text{HNO}_3} \approx 0.03$  Torr at 15 °C.

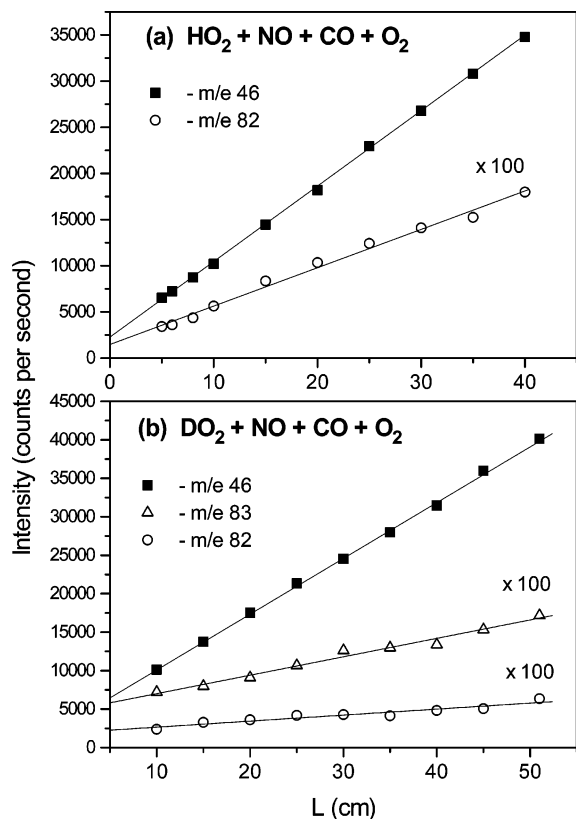


**Figure 2.** Chemical amplification in the HO<sub>2</sub>/NO/CO/O<sub>2</sub> (a) and HO<sub>2</sub>/NO/CO/O<sub>2</sub> (b) systems at 200 Torr and 298 K: (a) [HO<sub>2</sub>] = 4.8 × 10<sup>11</sup>, [NO] = 5.9 × 10<sup>13</sup>, [O<sub>2</sub>] = 1.8 × 10<sup>16</sup>, and [CO] = 2.2 × 10<sup>17</sup> molecule cm<sup>-3</sup> (chain length 5.6); (b) [DO<sub>2</sub>] = 8 × 10<sup>11</sup>, [NO] = 3 × 10<sup>13</sup>, [O<sub>2</sub>] = 1.2 × 10<sup>16</sup>, [CO] = 3 × 10<sup>17</sup> molecule cm<sup>-3</sup> (chain length 4.6).

Calibration of the NO<sub>2</sub> signal was made by flowing a commercial NO<sub>2</sub> gas mixture (Alpha Gaz, 5000 ppm in N<sub>2</sub>) into the TFR. The mixture flow rate was measured by a TYLAN-2900 mass flow controller. The NO<sub>2</sub> sensitivities,  $S_{\text{NO}_2}$ , were obtained from the slopes of the linear dependence of the signal intensity at  $m/e$  46 on the concentration calculated from the flow rate. The signal intensities were measured in the range of [NO<sub>2</sub>] = 3 × 10<sup>11</sup> to 2 × 10<sup>13</sup> molecule cm<sup>-3</sup> for which a good linearity was observed at each pressure. Similarly to HNO<sub>3</sub>, the pressure dependence was expressed relative to that at  $P = 200$  Torr,  $S_P/S_{200}(\text{NO}_2) = S_{\text{NO}_2}(P)/S_{\text{NO}_2}(200)$ . The sensitivities for NO<sub>2</sub> and HNO<sub>3</sub> exhibited different pressure dependences, which very likely resulted from different formation mechanisms of product ions. Both were found to decrease with increasing pressure in the TFR keeping all the other parameters unchanged as it was the case in these experiments. Finally, having made calibrations for NO<sub>2</sub> and HNO<sub>3</sub>, a pressure factor  $f_P = [S_P/S_{200}(\text{HNO}_3)]/[S_P/S_{200}(\text{NO}_2)]$  was determined for the calculation of the HNO<sub>3</sub> to NO<sub>2</sub> concentration ratio.

Change of the temperature in the TFR at a constant pressure has no noticeable influence on the signal intensities of NO<sub>2</sub> and HNO<sub>3</sub> as was shown in test experiments at 200 Torr. In these experiments, NO<sub>2</sub>-He and HNO<sub>3</sub>-He mixtures were continuously introduced into the reactor where the temperature was lowered from 300 to 239 K while constant pressure was maintained by regulating the reactor pumping.

### 3. Results

**3.1. Chemical Amplification of HNO<sub>3</sub> formation in the HO<sub>2</sub>/NO/CO/O<sub>2</sub> System.** Use of the chemical amplification (1a–3) in the TFR allowed an increase of the signal intensities

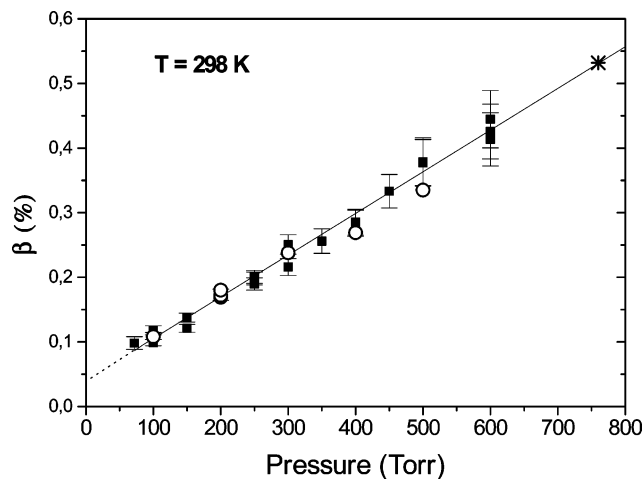
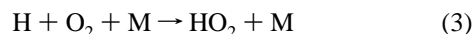
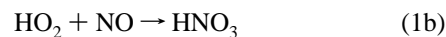
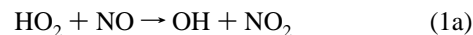


**Figure 3.** Pressure dependence of  $\beta = k_{1b}/k_{1a}$  at 298 K. Open circles denote measurements with chemical HNO<sub>3</sub> calibration; star is the extrapolation to atmospheric pressure (760 Torr).

of produced nitric acid that was a critical factor in reducing experimental uncertainties, and confirmation of the previously measured branching ratio  $k_{1a}/k_{1b}$ .<sup>1</sup> Amplification of the signal was achieved by adding into the TFR high concentrations of CO and O<sub>2</sub>, creating a chain mechanism that includes termination reaction 1b:



At the same time, CO in reaction (2) served as a scavenger of OH radicals preventing formation of nitric acid in the secondary reaction (4):



Figure 2a illustrates the increase of the NO<sub>2</sub> and HNO<sub>3</sub> concentrations with the increase of the distance  $L$  between the injector tip and the interface cone in the HO<sub>2</sub>/NO/CO/O<sub>2</sub> system. This run was done at  $P = 200$  Torr,  $T = 298$  K, and initial concentrations [HO<sub>2</sub>] = 4.8 × 10<sup>11</sup>; [NO] = 5.9 × 10<sup>13</sup>; [O<sub>2</sub>] = 1.8 × 10<sup>16</sup>; and [CO] = 2.2 × 10<sup>17</sup> molecule cm<sup>-3</sup>. The initial concentration of HO<sub>2</sub> was determined by measuring the NO<sub>2</sub> concentration formed in the reaction in the absence of CO. The maximum NO<sub>2</sub> concentration formed in the presence of CO was 2.8 × 10<sup>12</sup> molecule cm<sup>-3</sup>, corresponding to a chain length of 5.8. The chain length was regulated by NO concentration, the limiting step being reaction 1a. It was necessary to limit the chain length in order to make the rate of reaction (4) negligible and thus to control the rate ratio of reactions 4 and 2, which is the probability of HNO<sub>3</sub> formation in reaction 4. In the given example, for maximum distance  $L = 50$  this ratio was  $\alpha = k_4[\text{NO}_2]_{\text{tot}}/k_2[\text{CO}] = 1.8 \cdot 10^{-4}$ . [NO<sub>2</sub>]<sub>tot</sub> is the mean total NO<sub>2</sub> concentration in the reactor equal to [NO<sub>2</sub>]<sub>react</sub>/2 + [NO<sub>2</sub>]<sub>bgr</sub>, where [NO<sub>2</sub>]<sub>react</sub> is the NO<sub>2</sub> concentration produced in the reaction at maximum  $L$  and [NO<sub>2</sub>]<sub>bgr</sub> is the background concentration originating mainly from the NO inlet system. The rate constants  $k_2$  and  $k_4$  were taken from ref 6. A linear amplification was observed for both NO<sub>2</sub> and HNO<sub>3</sub> products described by the equations  $I_{46} = (814 \pm 11)L + 2282$  and  $I_{82}$

**TABLE 1: Determination of  $\beta = k_{1b}/k_{1a}$  at Different Pressures and 298 K Using Chemical Calibration of  $\text{HNO}_3^a$** 

P Torr	$N^b$	$S_{\text{NO}_2}^c$	$S_{\text{OH}}^c$	$S_{\text{HNO}_3}^c$	$\Delta I_{82}/\Delta I_{46}$ $10^{-4}$	$b_{82}/b_{46}^d$ $10^{-4}$	$\beta_{\text{int}}^e$ %	$\beta_{\text{slope}}^f$ %	$\alpha^g$ %
$10^{-8}$ cps/molecule $\text{cm}^{-3}$									
200	1	1.23	2.32	3.79	$51.9 \pm 2.8$	$51.5 \pm 1.8$	$0.169 \pm 0.023$	$0.167 \pm 0.022$	0.018
	2	1.74	3.31	7.63	$75.5 \pm 4.3$	$72.9 \pm 5.3$	$0.172 \pm 0.024$	$0.166 \pm 0.024$	0.019
	3	1.98	2.90	6.80	$61.7 \pm 5.5$	$63.6 \pm 5.6$	$0.180 \pm 0.028$	$0.185 \pm 0.030$	0.028
	4	0.93	1.67	6.67	$113 \pm 5.4$	$111 \pm 4.9$	$0.169 \pm 0.023$	$0.166 \pm 0.022$	0.016
Average:							$0.173 \pm 0.010$	$0.171 \pm 0.016$	
100	1	1.75	4.49	12.0	$74.2 \pm 4.5$	$73.1 \pm 4.8$	$0.108 \pm 0.015$	$0.107 \pm 0.016$	0.012
300	1	1.49	1.66	4.57	$73.1 \pm 3.5$		$0.238 \pm 0.037$		0.012
400	1	1.97	2.08	2.10	$28.7 \pm 3.9$		$0.269 \pm 0.043$		0.013
500	1	1.07	1.32	1.16	$37.4 \pm 4.0$	$35.0 \pm 3.8$	$0.345 \pm 0.077$	$0.345 \pm 0.074$	0.008

<sup>a</sup> Calibration using  $\text{H} + \text{NO}_2$  and  $\text{OH} + \text{NO}_2$  reactions. <sup>b</sup> Experiment number. <sup>c</sup>  $S_X$  denotes sensitivity to species X. <sup>d</sup>  $b_M$  is the slope of the linear dependence of signal intensity at  $m/e$  M versus reaction time. <sup>e</sup> Values from the intensities. <sup>f</sup> From the slopes. <sup>g</sup>  $\alpha = k_5[\text{NO}_2]_{\text{tot}}/k_3[\text{CO}]$  is the upper limit for the probability of  $\text{HNO}_3$  formation in the side  $\text{OH} + \text{NO}_2$  reaction.

$= (4.19 \pm 0.13)L + 14.8$ . The top panel of Table 1 presents the branching ratios calculated from this experiment (first line) and three other similar experiments carried out at 200 Torr with chemical calibration. In these experiments, the product intensity ratios,  $\Delta I_{82}/\Delta I_{46}$ , were determined both from the slopes of the amplification kinetics and by averaging the  $\Delta I_{82}/\Delta I_{46}$  values for different positions of the injector. The average value is  $\beta = (0.173 \pm 0.008)\%$ . Taking into account the systematic errors in calibration, the final result can be expressed as  $\beta = (0.17 \pm 0.03)\%$ .

Chemical amplification of the deuterated nitric acid,  $\text{DNO}_3$ , was obtained in the isotopic  $\text{DO}_2/\text{NO}/\text{CO}/\text{O}_2$  system, when the discharge in  $\text{D}_2/\text{He}$  mixture was used to produce D-atoms. Figure 2b shows the results of the kinetic measurements for  $\text{NO}_2$ ,  $\text{DNO}_3$  and  $\text{HNO}_3$  at  $P = 200$  Torr,  $T = 298$  K, and initial concentrations  $[\text{DO}_2] + [\text{HO}_2] = 9.5 \times 10^{11}$ ;  $[\text{NO}] = 2.9 \times 10^{13}$ ;  $[\text{O}_2] = 1.2 \times 10^{16}$ ;  $[\text{CO}] = 2.5 \times 10^{17}$  molecule  $\text{cm}^{-3}$ . Appearance of  $\text{HNO}_3$  ( $m/e = 82$ ) is explained by the formation of OH and H-atoms from the dissociation of  $\text{H}_2\text{O}$  traces in He carrier gas. The initial ratio of  $[\text{H}]/[\text{D}] = 0.14$  was obtained by the titration of the discharge products with  $\text{NO}_2$ . Isotopic  $\text{DNO}_3$  also exhibits linear kinetics proving that the nitric acid observed in the  $\text{HO}_2 + \text{NO}$  reaction is not a product of the surface reaction of  $\text{NO}_2$  with  $\text{H}_2\text{O}$ . Assuming similar sensitivities to  $\text{HNO}_3$  and  $\text{DNO}_3$ , the observed  $\text{DNO}_3$  signal intensity indicates that the branching ratio for the isotopic  $\text{DO}_2 + \text{NO}$  reaction would be a factor of  $\sim 2$  lower than for reaction 1.

**3.2. Pressure Dependence of the Branching Ratio at Room Temperature.** At room temperature, the kinetics of the formation of  $\text{NO}_2$  and  $\text{HNO}_3$  products were measured in the presence of CO as described above at different pressures ranging from 72 to 600 Torr. The bottom panel of Table 1 contains the results obtained using chemical calibration at 100, 300, 400, and 500 Torr and Table 2 contains the results from the six experiments with variable pressure using direct calibration of  $\text{HNO}_3$ . In most experiments, the  $\Delta I_{82}/\Delta I_{46}$  ratio was determined from the slopes of the amplification kinetics. Some experiments were done at a fixed  $L$  making several measurements of  $\text{NO}_2$  and  $\text{HNO}_3$  with the discharge switched on and off (experiment 5 in Table 2). The measured intensity ratios were corrected by sensitivity pressure factor  $f_P$  determined with respect to 200 Torr as described in the Experimental Section. Then, division of the corrected intensity ratios by that for 200 Torr gives  $\beta/\beta_{200}$ , the reaction branching ratio at a given pressure relative to that at 200 Torr which is a known value:

$$\beta(P) = [\Delta I_{82}/\Delta I_{46}(P)/\Delta I_{82}/\Delta I_{46}(200)]f_P\beta_{200} \quad (\text{Eq1})$$

**TABLE 2: Determination of the Pressure Dependence of  $\beta = k_{1b}/k_{1a}$  at 298 K Using Sensitivity Pressure Factor<sup>a</sup>**

$N^b$	P Torr	$[\text{NO}_2]_{\text{bgr}}$ $10^{11}$	$\Delta[\text{NO}_2]$ $10^{12}$	$[\text{CO}]$ $10^{17}$	$f_P^a$	$\Delta I_{82}/\Delta I_{46}$ $10^{-4}$	$\beta/\beta_{200}^c$	$\beta$ %	$\alpha^d$ %
1	100	1.6	2.0	1.9	0.62	47.7	0.57	0.097	0.012
	150	2.4	2.5	2.2	0.73	49.7	0.70	0.118	0.020
	<b>200</b>	<b>2.7</b>	<b>2.5</b>	<b>2.5</b>	<b>1</b>	<b>51.9</b>	<b>1</b>	<b>0.169</b>	0.017
2	<b>200</b>	<b>4.0</b>	<b>4.2</b>	<b>2.5</b>	<b>1</b>	<b>61.7</b>	<b>1</b>	<b>0.180</b>	<b>0.028</b>
	250	3.9	3.0	2.8	1.24	57.0	1.15	0.206	0.020
	300	3.6	2.3	3.1	1.61	55.5	1.45	0.261	0.016
	350	4.2	0.54	3.3	2.12	47.1	1.62	0.280	0.008
3	<b>200</b>	<b>2.0</b>	<b>2.4</b>	<b>2.1</b>	<b>1</b>	<b>75.5</b>	<b>1</b>	<b>0.173</b>	<b>0.018</b>
	400	4.2	1.6	3.2	2.55	47.4	1.64	0.282	0.012
	500	4.2	1.1	3.5	3.60	46.1	2.19	0.378	0.010
	600	4.8	0.43	3.4	4.59	42.1	2.57	0.441	0.008
4	<b>200</b>	<b>1.9</b>	<b>2.4</b>	<b>2.4</b>	<b>1</b>	<b>57.0</b>	<b>1</b>	<b>0.173</b>	<b>0.016</b>
	600	4.7	0.72	6.0	4.59	30.5	2.45	0.425	0.005
5	172	2.3	3.3	2.7	0.73	40.8	0.95	0.164	0.018
	<b>200</b>	<b>2.4</b>	<b>2.8</b>	<b>2.7</b>	<b>1</b>	<b>34.3</b>	<b>1</b>	<b>0.173</b>	<b>0.017</b>
	250	1.8	1.4	2.3	1.24	32.0	1.16	0.201	0.013
	300	2.4	1.6	2.8	1.61	26.5	1.25	0.216	0.012
	350	3.0	1.4	3.3	2.16	23.5	1.48	0.256	0.012
	400	3.6	1.7	3.7	2.61	21.7	1.65	0.285	0.012
	500	3.6	1.1	3.5	3.71	20.1	2.18	0.377	0.010
600	4.3	0.78	4.2	4.59	17.8	2.39	0.413	0.008	
6	72	1.3	1.3	2.5	0.51	48.4	0.57	0.098	0.005
	100	1.6	2.3	2.5	0.62	48.1	0.68	0.118	0.010
	150	2.2	3.0	2.5	0.73	43.8	0.76	0.132	0.017
	<b>200</b>	<b>3.5</b>	<b>4.6</b>	<b>3.7</b>	<b>1</b>	<b>43.6</b>	<b>1</b>	<b>0.173</b>	<b>0.020</b>
	250	2.9	4.1	4.0	1.24	41.0	1.10	0.189	0.019
	450	2.7	1.5	7.2	1.81	27.7	1.95	0.337	0.006

<sup>a</sup> See Experimental Section for determination of pressure correction factor  $f_P$  using external source of  $\text{HNO}_3$ . <sup>b</sup> Experiment number. <sup>c</sup> Branching ratio with respect to that at 200 Torr. <sup>d</sup> Upper limit for the probability of  $\text{HNO}_3$  formation in the  $\text{OH} + \text{NO}_2$  side reaction. Concentrations are in molecule  $\text{cm}^{-3}$ .

The obtained pressure dependence is shown in Figure 3. It is a linear function of pressure expressed by

$$\beta(P) = (6.4 \pm 0.3) \times 10^{-4}P(\text{Torr}) + (4.2 \pm 0.8) \times 10^{-2} \quad (\text{Eq2})$$

with  $2\sigma$  uncertainty limits. Extrapolation to atmospheric pressure gives  $\beta(760) = 0.53\%$ , which is indicated by a star symbol in Figure 3. It is worth noting that the obtained dependence has a positive zero intercept. Assuming  $\beta \rightarrow 0$  when  $P \rightarrow 0$ , the measurements indicate that there should be a nonlinear dependence at low pressures.

**3.3. Temperature Dependence of the Branching Ratio at Different Pressures.** Temperature dependence of  $\beta$  was measured by keeping a constant mass flow rate of the carrier gas and the reactants at a given pressure. The constant pressure

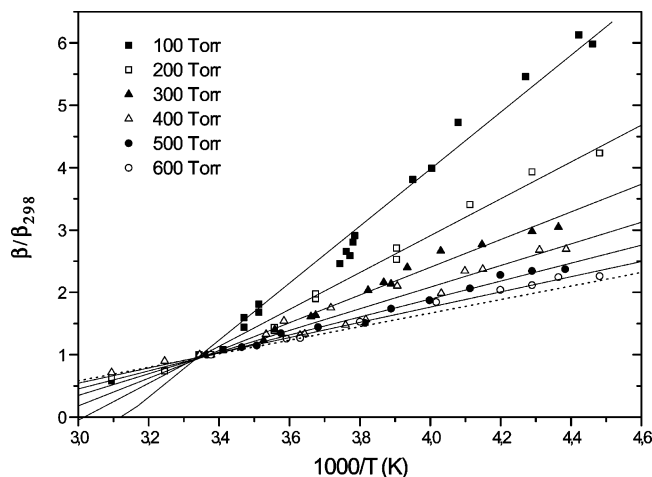


**Figure 4.** Normalized temperature dependence of  $\beta = k_{1b}/k_{1a}$  at different pressures. Dotted line is the extrapolation to 760 Torr.

during the cooling was maintained by regulating the throttling valve of the reactor pump. As a rule, the measurements were done at a fixed position of the injector, corresponding to  $L = 50$  cm. Table 3 gives the measured signal intensity ratios and the ratios normalized to the room-temperature value, which is identical to the normalized branching ratio,  $\beta/\beta_{298}$ . The concentrations of NO, O<sub>2</sub>, and CO given in Table 3 correspond to  $T = 298$  K. Figure 4 presents a summary of the normalized branching ratios as a function of  $1000/T$ . The observed plots could be rather well approximated by a linear fit. These fits are shown in Figure 4 by solid lines (the data obtained above 298 K were excluded from the linear regression analysis). The slopes of the linear fit monotonically decrease with the increase of

pressure. The extrapolation to atmospheric pressure (black dotted line) was obtained from the power function fit for this decrease.

When the normalized temperature curve for every pressure is multiplied by the corresponding  $\beta$  coefficient given by eq 1, we obtain a full picture for the branching ratio, as shown in Figure 5. In the 298–223 K range temperature dependences for different pressures present a set of nearly parallel and equidistant straight lines. The linear fit fails at temperatures higher than 298 K, where curvatures were observed for  $P = 100, 200,$  and  $400$  Torr. Below 298 K the whole set of data can be described by the simple three-parameter expression of the general form

$$\beta(P, T) = a/T + bP + c \quad (\text{Eq3})$$

Coefficient  $a$  was found by averaging the slopes of the observed temperature dependencies, coefficients  $b$  and  $c$  were determined by standard two-parameter least-square fit of the data. The numerical expression can be written as

$$\beta(P, T) = (530 \pm 20)/T(\text{K}) + (6.4 \pm 1.3) \times 10^{-4}P(\text{Torr}) - (1.73 \pm 0.07) \quad (\text{Eq4})$$

(with  $2\sigma$  uncertainties). In Figure 6 the pressure dependence for HNO<sub>3</sub> production is reported at four temperatures: 298, 263, 249, and 228 K, with the nearest available experimental points taken in the vicinity of these temperatures. The straight lines were calculated using eq 4. Extrapolated to zero pressure, they exhibit larger intercepts for lower temperatures.

#### 4. Discussion

Recently, a theoretical examination of the mechanisms on the HNO<sub>3</sub> potential energy surface ( $\text{HO}_2 + \text{NO} \rightleftharpoons \text{HOONO} \rightleftharpoons$

**TABLE 3: Measurement of the Temperature Dependence of  $\beta = k_{1b}/k_{1a}$  at Different Pressures**

$T$ K	$\Delta I_{82}/\Delta I_{46}$ $10^{-4}$	$\beta/\beta_{298}^a$	$T$ K	$\Delta I_{82}/\Delta I_{46}$ $10^{-4}$	$\beta/\beta_{298}^a$	$T$ K	$\Delta I_{82}/\Delta I_{46}$ $10^{-4}$	$\beta/\beta_{298}^a$
$P = 100$ Torr; $[\text{NO}] = 4.1 \times 10^{13}$ ; $[\text{O}_2] = 1.4 \times 10^{16}$ ; $[\text{CO}] = 2.4 \times 10^{17}$ molecule $\text{cm}^{-3}$								
298	113	1	265	311	2.74	226	695	6.13
293	123	1.08	253	432	3.81	223	678	5.98
288	172	1.52	249	452	4.00	298	97.1	1
285	198	1.75	245	536	4.73	308	71.8	0.74
267	279	2.46	234	618	5.45	323	56.5	0.58
$P = 200$ Torr; $[\text{NO}] = 3.8 \times 10^{13}$ ; $[\text{O}_2] = 1.2 \times 10^{16}$ ; $[\text{CO}] = 2.5 \times 10^{17}$ molecule $\text{cm}^{-3}$								
298	38.7	1	243	132	3.41	298	33.7	1
281	53.0	1.45	233	152	3.93	308	24.9	0.74
272	76.4	1.98	223	164	4.24	323	21.3	0.63
256	105	2.71						
$P = 300$ Torr; $[\text{NO}] = 5.4 \times 10^{13}$ ; $[\text{O}_2] = 1.6 \times 10^{16}$ ; $[\text{CO}] = 2.9 \times 10^{17}$ molecule $\text{cm}^{-3}$								
298	25.0	1	261	51.0	2.03	241	69.4	2.77
283	30.8	1.23	257	53.5	2.14	233	75.1	2.98
281	35.1	1.40	254	60.1	2.40	229	76.3	3.05
273	40.3	1.61	248	65.1	2.53			
$P = 400$ Torr; $[\text{NO}] = 6.1 \times 10^{13}$ ; $[\text{O}_2] = 2.1 \times 10^{16}$ ; $[\text{CO}] = 3.5 \times 10^{17}$ molecule $\text{cm}^{-3}$								
298	31.5	1	256	66.1	2.10	228	84.7	2.69
283	41.8	1.33	250	62.5	1.99	298	16.2	1
279	48.0	1.53	241	74.2	2.36	308	14.6	0.90
266	46.6	1.48	232	84.4	2.68	323	11.6	0.72
$P = 500$ Torr; $[\text{NO}] = 9 \times 10^{13}$ ; $[\text{O}_2] = 2.7 \times 10^{16}$ ; $[\text{CO}] = 4.8 \times 10^{17}$ molecule $\text{cm}^{-3}$								
298	14.2	1	272	20.5	1.44	243	29.4	2.07
289	16.0	1.12	262	24.7	1.74	238	32.4	2.28
285	16.3	1.15	255	21.5	1.51	233	33.3	2.34
280	20.2	1.42	250	26.6	1.87	228	33.8	2.37
$P = 600$ Torr; $[\text{NO}] = 4.0 \times 10^{13}$ ; $[\text{O}_2] = 3.2 \times 10^{16}$ ; $[\text{CO}] = 4.0 \times 10^{17}$ molecule $\text{cm}^{-3}$								
298	18.9	1	263	28.9	1.53	233	40.0	2.12
278	23.8	1.26	249	34.9	1.85	229	42.5	2.25
275	24.0	1.27	238	38.6	2.04	223	42.8	2.26

<sup>a</sup> Branching ratio with respect to that at 298 K.

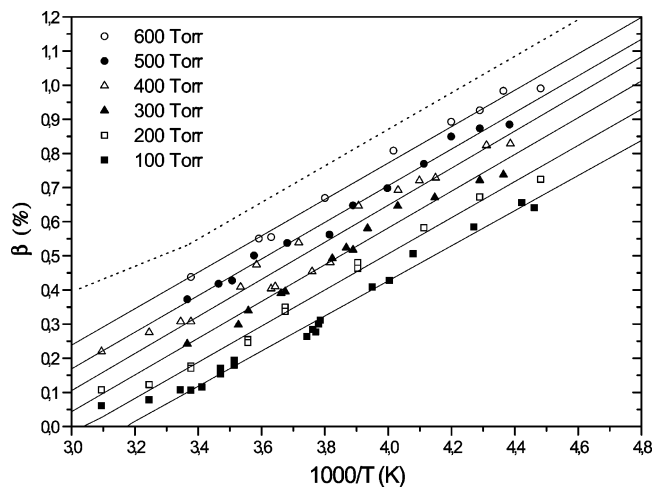


**Figure 5.** Pressure and temperature dependences of  $\beta = k_{1b}/k_{1a}$ . Upper dotted line represent extrapolation to  $P = 760$  Torr.

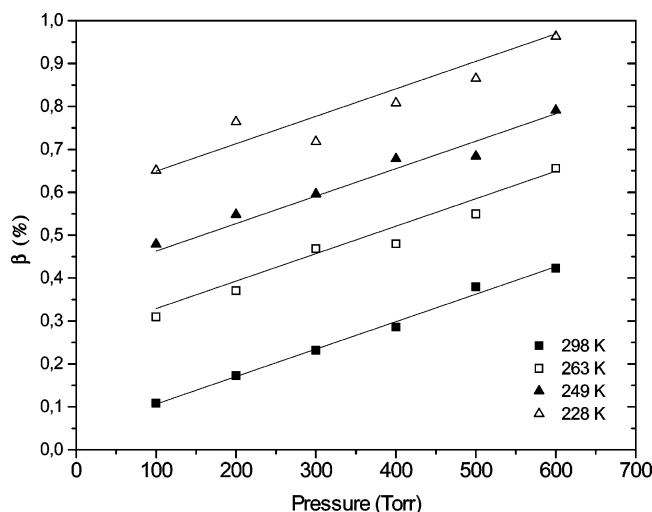


**Figure 6.** Pressure dependence of  $\beta = k_{1b}/k_{1a}$  at different temperatures. Solid curves correspond to eq 3.

$\text{OH} + \text{NO}_2 \rightleftharpoons \text{HNO}_3$ ) has been performed by Zhang and Donahue using a multiple-well master-equation simulation of the system.<sup>7</sup> To constrain the parameters of the simulation, the authors used the experimental evidence for  $\text{HNO}_3$  production in the  $\text{HO}_2 + \text{NO}$  reaction,<sup>1</sup> the experimental data on formation and decay of *cis*- and *trans*-conformers of the short-lived HOONO intermediate in the  $\text{OH} + \text{NO}_2$  reaction,<sup>8–10</sup> and on isotopic scrambling in  $^{18}\text{OH} + \text{NO}_2$ .<sup>10,11</sup> The calculations show that channel 1b can occur by isomerization of *trans*-HOONO to HONO<sub>2</sub>, if a high barrier between *cis* and *trans* conformers and a low barrier for isomerization to HONO<sub>2</sub> are assumed. A good agreement with our branching fraction for  $\text{HNO}_3$  formation in reaction 1 at 298 K<sup>1</sup> was obtained with the energy of the transition state for isomerization of approximately 5 kcal mol<sup>-1</sup> lower than the energy of  $\text{OH} + \text{NO}_2$ . The existence of such a low-lying “rotational” transition state was first proposed by Dransfield et al.<sup>12</sup> A search for the transition states for HOONO rearrangements was performed by Zhao et al.<sup>13</sup> using density functional theory. The authors suggest that O–O cleavage in HOONO may lead to hydrogen-bonded  $\text{OH}\cdots\text{ONO}$  complexes which through rotational motion can be reoriented for N–O bond formation and collapse to HONO<sub>2</sub>. The complexes and the transition states for isomerization were located at the B3LYP/6-311++G\*\* and CBS-QB3 levels. All these stationary points were found to be very similar in energy, in the range of 1–2

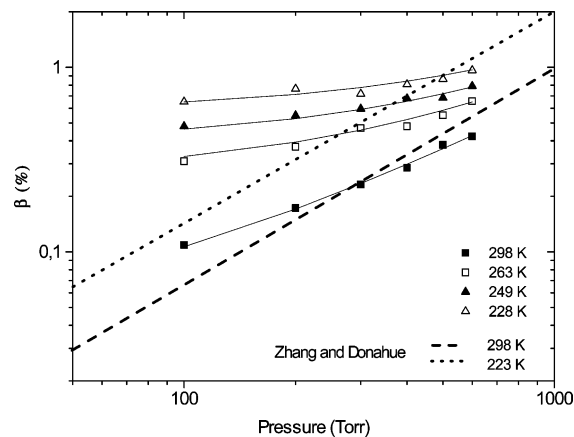


**Figure 7.** Representation of the Figure 6 in logarithmic scale for comparison with the calculation from Zhang and Donahue<sup>9</sup> (thick curves).

kcal mol<sup>-1</sup> lower than the free OH and NO<sub>2</sub>. However, in contrast to ref 9, where the isomerization path was involved to explain the observed decay of *trans*-HOONO, Zhao et al. believe that the isomerization occurs easier from *cis*-HOONO than from *trans*-HOONO conformation.

According to theoretical considerations,<sup>7</sup> the pressure dependences in Figure 6 can be interpreted as a falloff corresponding to stabilization of the excited HONO<sub>2</sub> formed at the  $\text{HO}_2 + \text{NO}$  energy. In Figure 7 we compare our present experimental results with the calculated pressure dependence<sup>7</sup> presented in logarithmic coordinates. As already mentioned, there is a rather good agreement between the measurements and theory at 298 K, although the theoretical pressure dependence at 298 K is somewhat steeper than the observation. As seen in Figure 7, the linearity of eq 1 breaks when switching to logarithmic scale because, formally,  $\beta \neq 0$  at zero pressure. Accordingly, the divergence between the measurements and calculations increases at lower temperatures because of larger intercepts. To summarize, theory does not exclude formation of HNO<sub>3</sub> in reaction 1; at ambient temperature, the observed pressure dependence of  $\beta$  can be reproduced by calculations in a limited pressure range (100–600 Torr). Also, calculations confirm the observed negative temperature dependence of  $\beta$ .

## 5. Atmospheric Implication

The obtained results confirmed our previous finding of a minor HNO<sub>3</sub> forming channel in the  $\text{HO}_2 + \text{NO}$  reaction, with an increase of the HNO<sub>3</sub> yield with decreasing temperature.<sup>1</sup> In addition, they show an increase of this yield with increasing pressure. The atmospheric consequences of this new process has been already considered in our previous paper, predicting a noticeable effect of reaction 1b on the concentrations of HO<sub>x</sub>, NO<sub>x</sub>, and ozone in the upper troposphere.<sup>1</sup> The plots of Figure 5 show a change of  $\beta = k_{1b}/k_{1a}$  roughly from 0.5% near the Earth’s surface (298 K, 760 Torr) to 0.8% in the tropopause region (220 K, 200 Torr). This suggests that reaction 1b could also have a significant effect in the middle and lower troposphere. The effect of reaction 1b on the atmospheric composition can be quantified by including this reaction in atmospheric models with the rate constant calculated using eq 4. Such model calculations have already been done using both 2D and 3D models.<sup>14</sup> The resulting impact of reaction 1b on the chemical composition of the troposphere could even be more significant considering the positive influence of water vapor on the branching ratio  $\beta$  which has been observed in the previous test experiments.<sup>1</sup> This humidity effect is going to be investigated

in more details by measuring  $\beta$  as a function of H<sub>2</sub>O concentration in extended ranges of pressure and temperature.

**Acknowledgment.** The work was carried out within the SCOUT project of the European Union and the National Programmes of Atmospheric Chemistry of CNRS (PNCA and LEFE-CHAT).

### References and Notes

- (1) Butkovskaya, N. I.; Kukui, A.; Pouvesle, N.; Le Bras, G. *J. Phys. Chem. A* **2005**, *109*, 6509.
- (2) Ikezoe, Y.; Matsuoka, S.; Takebe, M.; Viggiano, A. *Gas Phase Ion-Molecule Reaction Rate Constants Through 1986*; Ion Reaction Research Group of the Mass Spectroscopy Society of Japan, Maruzen Company: Tokyo, Japan, 1987.
- (3) Elrod, M. J.; Ranschaert, D. L.; Schneider, N. J. *Int. J. Chem. Kinet.* **2001**, *33*, 363.
- (4) Huey, L. G.; Hanson, D. R.; Howard, C. J. *J. Phys. Chem.* **1995**, *99*, 5001.
- (5) Okumura, M.; Sander, S. P.; Sivakumaran, V.; Mollner, A. K.; Fry, J. L.; Feng, L. *Gas-Phase Formation Rates of Nitric Acid and its Isomers under Urban Conditions*; Final Report to California Air Resources Board, CARB Contract No. 03-333; California Air Resources Board: Sacramento, CA, 2005.
- (6) Sander, S. P.; Friedl, R. R.; Golden, D. M.; Kurylo, M. J.; Moortgat, G. K.; Wine, P. H.; Ravishankara, A. R.; Kolb, C. E.; Molina, M. J.; Finlayson-Pitts, B. J.; Huie, R. E.; Orkin, V. L. *Chemical Kinetics and Photochemical Data for Use in Atmospheric Studies*; JPL Publication 06-2, Evaluation Number 15; Jet Propulsion Laboratory: Pasadena, CA, 2006.
- (7) Zhang, J.; Donahue, N. M. *J. Phys. Chem. A* **2006**, *110*, 6898.
- (8) Hippler, H.; Nasterlack, S.; Striebel, F. *Phys. Chem. Chem. Phys.* **2002**, *4*, 2959.
- (9) Fry, J. L.; Nizkorodov, S. A.; Okumura, M.; Roehl, C. M.; Francisco, J. S. *J. Chem. Phys.* **2004**, *121*, 1432.
- (10) D'Ottone, L.; Bauer, D.; Campuzano-Jost, P.; Fardy, M.; Hynes, A. J. *Faraday Discuss.* **2005**, *130*, 1.
- (11) Donahue, N. M.; Mohrschladt, R.; Dransfield, T. J.; Anderson, J. G.; Dubey, M. K. *J. Phys. Chem. A* **2001**, *105*, 1515.
- (12) Dransfield, T. J.; Donahue, N. M.; Anderson, J. G. *J. Phys. Chem. A* **2001**, *105*, 1507.
- (13) Zhao, Y.; Houk, K. N.; Olson, L. P. *J. Phys. Chem. A* **2004**, *108*, 5864.
- (14) Chipperfield, M. P.; Evans, M. J.; Cariolle, D.; Butkovskaya, N. I.; Kukui, A.; Le Bras, G. Manuscript in preparation.